

The growth and characterization of layered, binary thin-film oxides: MgO–NiO and CaO–NiO

C. Xu, W. S. Oh, Q. Guo, and D. W. Goodman
Department of Chemistry, Texas A&M University, College Station, Texas 77843

(Received 11 October 1995; accepted 18 March 1996)

Layered, binary thin-film oxides of NiO, MgO and CaO have been prepared and characterized using low energy electron diffraction, Auger electron spectroscopy, energy loss spectroscopy, ion scattering spectroscopy, and temperature programmed desorption using probe molecules. Epitaxial growth was observed for the NiO–MgO and CaO–NiO systems; however, superior wetting was found for NiO–MgO relative to CaO–NiO. The thermal stabilities of the supported monolayer oxide vary significantly for the four systems studied, i.e. NiO/MgO, NiO/CaO, MgO/NiO and CaO/NiO, with NiO/CaO having the lowest thermal stability and CaO/NiO, the highest. © 1996 American Vacuum Society.

I. INTRODUCTION

The interface between two oxides is important in a number of technologies including those related to ceramics, electronic devices and catalysis.^{1–5} Supported oxides, which are widely used as catalysts, often show widely varying properties depending upon the particular support. A microscopic understanding of the nature of the interaction at oxide/oxide interfaces will undoubtedly aid in the design and improvement of mixed-oxide materials. Recently, we have demonstrated that thin oxide films grown epitaxially on refractory metal substrates can be used conveniently in surface science studies.^{6–15} These thin oxide films are thick enough (~ 100 Å) to simulate the chemical and physical properties of the terminated bulk oxide, yet sufficiently conductive (thermally and electrically) to circumvent the usual difficulties associated with the application of charged-particle probes to the corresponding bulk materials. In this paper, this thin-film approach to studying oxides is extended to layered mixed-oxides.

NiO, MgO and CaO crystallize in the rocksalt structure. NiO and MgO have very similar lattice parameters, while that of CaO is considerably larger. How the lattice constant mismatch influences the growth and stability of the mixed layered oxides is one of the questions to be addressed in this study. The single component oxide surfaces have been studied extensively in our laboratories and by others.^{16,17} These previous investigations provide an excellent reference from which to initiate the present studies.¹⁸

II. EXPERIMENT

The experiments were carried out in two ultrahigh vacuum (UHV) chambers. One is equipped with a LK2000 spectrometer for high resolution electron energy loss spectroscopy (HREELS) and energy loss spectroscopy (ELS), a single pass cylindrical mirror analyzer for Auger electron spectroscopy (AES), four-grid optics for low energy electron diffraction (LEED), and a quadrupole mass spectrometer (QMS) for temperature programmed desorption (TPD). The second chamber is equipped with capabilities for TPD and

LEED, and with a hemispherical analyzer for x-ray photoelectron spectroscopy (XPS), ion scattering spectroscopy (ISS) and AES. The base pressure of these systems was $\sim 3 \times 10^{-10}$ Torr.

TPD experiments were carried out using a line-of-sight QMS and a linear heating rate of 5 K/s. The ELS spectra were acquired in the specular direction with an electron incident angle of 60° with respect to the surface normal. An electron beam energy of 25 eV was used with a typical resolution of 25 meV. The ISS experiments were performed with a He⁺ beam energy of 600 eV. A differentially pumped ion gun was used in the raster mode to minimize any possible beam damage during the ISS experiments.

A Mo(100) surface was used to support the mixed oxide films and was cleaned by annealing in 1×10^{-8} Torr O₂ at 1200 K with a subsequent flash to 2000 K. This procedure was repeated several times until no contamination could be detected with AES. The oxide films were prepared by depositing the precursor metal at substrate temperatures between 300 and 500 K in a controlled O₂ background pressure, followed by annealing in 1×10^{-6} Torr of O₂. The metal source was extensively outgassed prior to use, and the metal flux calibrated using TPD and/or AES of the corresponding metal on the Mo(100) surface. For Mg and Ca, well-defined features for monolayer and multilayer desorption are apparent in the TPD spectra, and can be conveniently used to estimate the metal coverages. For Ni on Mo(100), the monolayer desorption peak cannot be cleanly resolved from the multilayer desorption peak, therefore, AES was used to estimate the Ni coverages and to calibrate the Ni flux.

III. RESULTS

A. Growth mode of the overlayer oxide

LEED was used to monitor the long-range order during the growth of the layered oxide films. For the Mo(100) surface, epitaxial NiO(100), MgO(100) and CaO(100) thin films were prepared as described previously.^{6–17} Onto these oxide films, a second oxide was deposited. A (1×1) square LEED pattern was observed for 0–30 ML of NiO on MgO(100) and

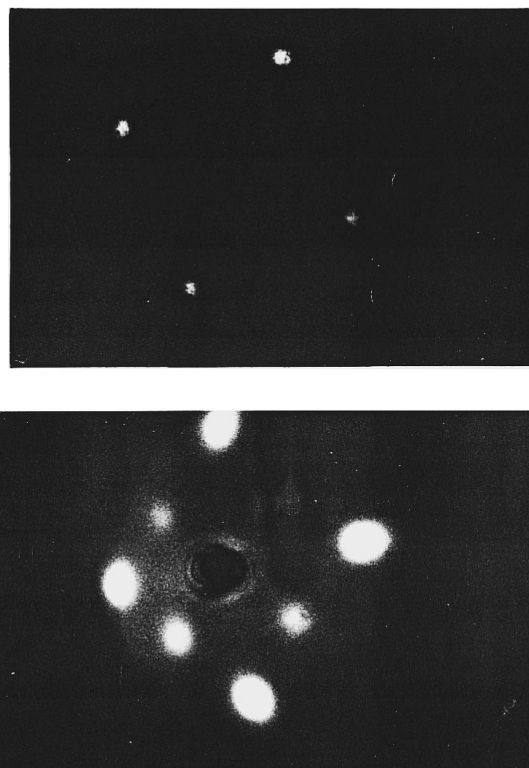


Fig. 1. LEED patterns of 18 ML of NiO on 20 ML of MgO(100)/Mo(100) surface (top), $E_p=62.3$ eV; and 20 ML of NiO on 30 ML of CaO/Mo(100) surface (bottom), $E_p=85$ eV.

CaO(100)/Mo(100), 0–30 ML of MgO on NiO(100)/Mo(100), and 0–30 ML of CaO on NiO(100)/Mo(100). Figure 1 shows two representative LEED patterns acquired for 18 ML of NiO on a 20 ML of MgO(100)/Mo(100) surface, and 20 ML of NiO on a 30 ML CaO(100)/Mo(100) surface. In both cases, a (1×1) LEED pattern was observed, with NiO on CaO(100) having much more diffuse spots than those observed for NiO on MgO(100). These data demonstrate that NiO grows epitaxially on the MgO(100) and CaO(100) surfaces, and likewise does CaO and MgO on the NiO(100) surface. It is noteworthy that NiO grown on MgO(100) as well as MgO grown on NiO(100) exhibit higher quality LEED patterns compared to the patterns observed for the corresponding oxide grown directly on the Mo(100) surface. This can be attributed to the closer lattice match between MgO and NiO compared to the match between either oxide and the Mo(100) surface.

To probe the growth mode in the monolayer regime, ISS spectra were taken as a function of the overlayer coverage. In Fig. 2, the relative ISS intensity of the substrate oxide is plotted versus the coverage of the overlayer oxide for NiO on MgO(100), MgO on NiO(100), CaO on NiO(100) and NiO on CaO(100). The single component oxide films were used to calibrate the relative sensitivities of Ni, Mg and Ca in the ISS. As shown in Fig. 2, NiO on MgO exhibits an identical behavior with respect to the substrate oxide ISS intensity versus coverage as seen for MgO on NiO. On the other hand, NiO on CaO and CaO on NiO show a separate and identical

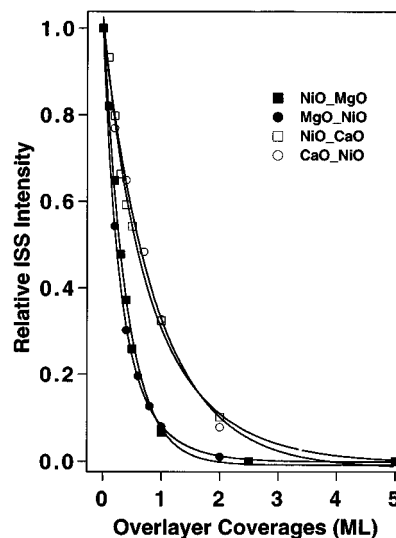


Fig. 2. ISS substrate oxide relative intensities versus overlayer oxide coverages for NiO/MgO, MgO/NiO, NiO/CaO, and CaO/NiO.

growth mode. However, the Ni (or Mg) ISS intensity attenuates more rapidly with respect to increasing MgO (or NiO) coverage than does the Ni (or Ca) ISS intensity with respect to the CaO (or NiO) coverage. For example, at an overlayer coverage of 1 equivalent monolayers (ML) in each case, the substrate oxide surfaces are ~90% covered for NiO/MgO(100) and MgO/NiO(100), while only ~65% covered for the CaO/NiO(100) and NiO/CaO(100). These results demonstrate clearly superior wetting between NiO and MgO compared to the wetting between NiO and CaO. These data indicate that NiO (or MgO) grows essentially layer-by-layer on the MgO(100) [or NiO(100)] surface within the first layer, while significant three dimensional clustering occurs within the first layer for CaO on NiO(100) and NiO on CaO(100) systems.

Figure 3 shows a TPD spectrum acquired following a saturation exposure of NO adsorption to a MgO_{0.8ML}/NiO(100)/Mo(100) surface. Two desorption features are evident at 120 and 200 K. The peak at 120 K is assigned to NO adsorbed on the MgO surface, while the peak at 200 K corresponds to NO adsorbed on the uncovered NiO sites. The well-resolved desorption peaks in Fig. 3 corresponding to NO on MgO and NiO provide a straightforward method for titrating the exposed NiO sites. It should be noted, however, that the area under the low-temperature NO features in the TPD of Fig. 3 does not correspond directly to the number of available MgO sites. This is due to the fact that the adsorption temperature (~100 K) used in these experiments is insufficient to fully saturate the coverage of NO on MgO.

The TPD area of NO on NiO was used to monitor the growth mode of MgO on NiO(100)/Mo(100) and CaO on NiO(100)/Mo(100) (Fig. 4). The decrease of the available NiO sites determined by the NO-TPD with increasing MgO (or CaO) coverages was identical to that found by ISS. As with the ISS results, more extensive two-dimensional growth

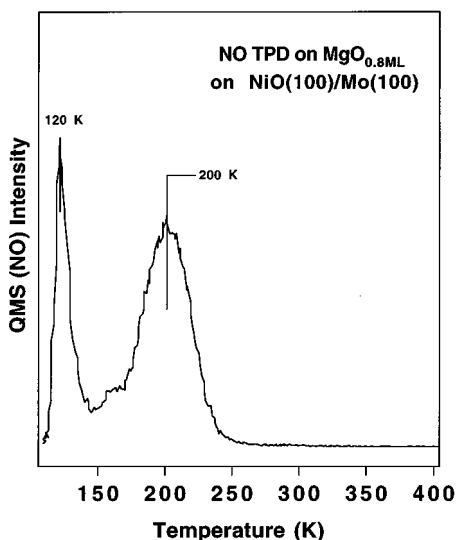


FIG. 3. NO-TPD acquired after a saturation NO exposure to a $MgO_{0.8ML}/NiO(100)/Mo(100)$ surface at 100 K.

was found for MgO on NiO(100) compared to CaO on NiO(100).

B. Thermal stability of mixed-oxide interfaces

The thermal stability of the mixed-oxide interfaces was studied using ISS and NO-TPD. Figure 5 shows two series of representative ISS spectra of $NiO_{1ML}/CaO(100)/Mo(100)$ and $CaO_{1ML}/NiO(100)/Mo(100)$ acquired after annealing to the indicated temperature. Three peaks are apparent at 273, 435 and 487 eV, corresponding to ion scattering from O, Ca and Ni. Figure 5 shows dramatic changes for NiO on

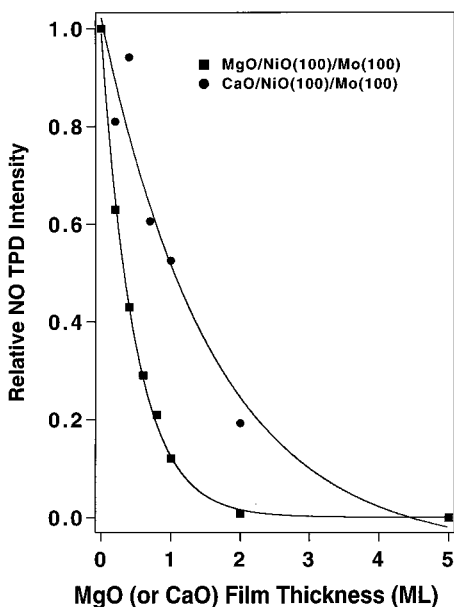


FIG. 4. Relative NO-TPD areas from the NiO substrate as a function of overlayer oxide coverages.

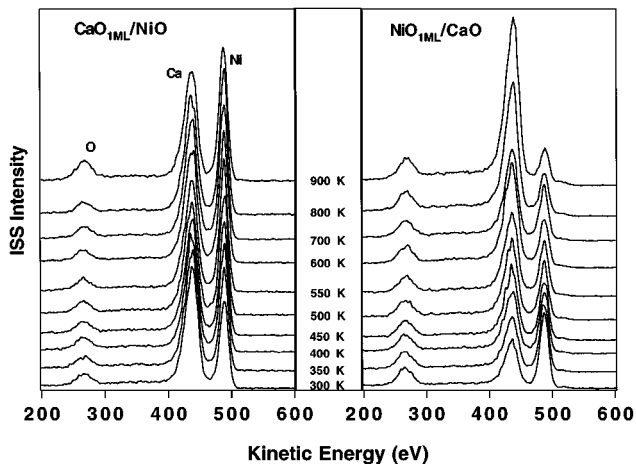


FIG. 5. ISS spectra of $CaO_{1ML}/NiO(100)$ (left) and $NiO_{1ML}/CaO(100)$ (right) taken after annealing to the indicated temperatures.

CaO(100) with annealing, while little change is apparent for CaO on NiO(100) upon heating. These results indicate a higher thermal stability for the CaO on NiO(100) compared to NiO on CaO(100). In Fig. 6 the relative ISS peak intensities of the substrate cations are plotted as a function of the annealing temperature for each of the systems studied. For $MgO_{1ML}/NiO(100)$ and $NiO_{1ML}/MgO(100)$, the relative substrate ISS intensity increases only slightly with annealing to 700 K. This slight increase is most likely due to a change in the overlayer morphology. Above 800 K, a large increase is evident, indicating significant interdiffusion of the overlayer and substrate oxides. The relative Ni-ISS intensities in the CaO/NiO(100) system increase slightly upon heating to 550 K, and can be attributed to subtle changes in the morphology of the overlayer CaO. Further annealing to 900 K causes virtually no change in the relative Ni-ISS intensity. That is, no significant interdiffusion with heating is indicated for

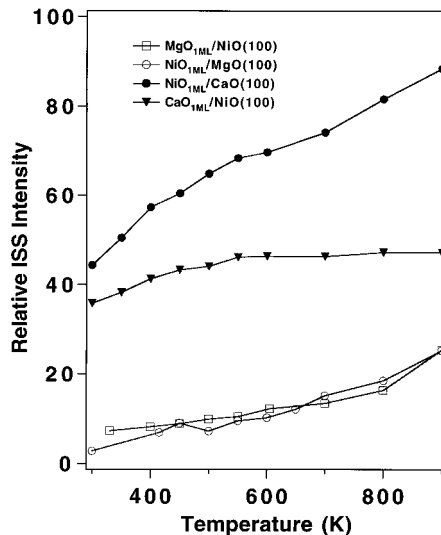


FIG. 6. Stabilities of various oxide/oxide interfaces with temperature probed with ISS (left) and NO-TPD (right).

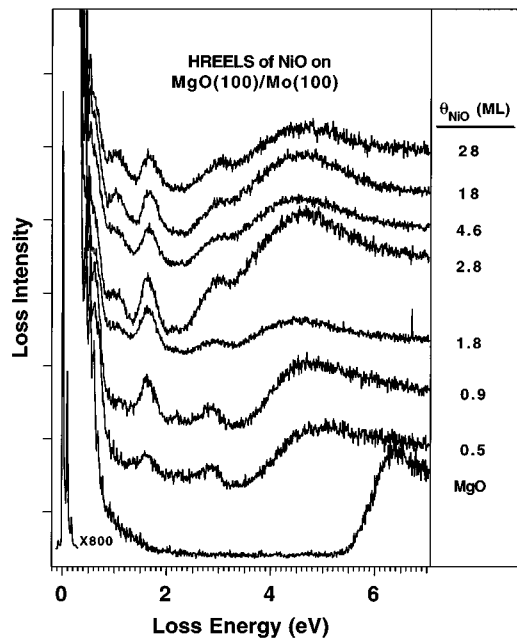


FIG. 7. Electron energy loss spectra of NiO films with various thicknesses on a 20 ML MgO(100)/Mo(100) substrate. $E_p = 25$ eV.

CaO/NiO(100). For NiO on CaO(100), significant interdiffusion has already occurred at 400 K. Using these results as a basis, the four systems investigated in our experiments can be placed into the following order of decreasing interface stability: CaO/NiO(100) > MgO/NiO(100) \approx NiO/MgO(100) > NiO/CaO(100).

C. Electronic structure of the overlayer oxide

To probe the electronic structure of thin NiO films supported on MgO(100), electron energy loss spectra (ELS) were acquired for various NiO film thicknesses (Fig. 7). The loss spectrum of a clean MgO(100)/Mo(100) surface (bottom curve, Fig. 7) exhibits a featureless baseline from 1 to ~ 5.5 eV, providing an ideal window for investigating the electronic structure of an overlayer NiO film. The loss peak at 6.5 eV in the MgO loss spectrum is assigned to the surface-related interband transition associated with the reduced coordination of the surface atoms compared to the bulk. This energy is considerably less than the 7.8 eV band gap of MgO.¹⁸ After the addition of 0.5 ML of NiO to the MgO(100)/Mo(100) surface, two intense peaks appear at 1.60 and 2.80 eV. In addition, a small peak at 2.20 eV and a very broad peak at 4.80 eV are apparent. No three-dimensional (3D) clustering is observed for 0.5 ML of NiO in the ISS and NO-TPD experiments, therefore the observed features can be assigned to a surface or interface state of NiO. Upon increasing the NiO coverage to 0.9 ML, the features at 1.60, 2.20, and 2.80 eV gain intensity and shift slightly to higher loss energy. A new feature at 1.10 eV also appears at 0.9 ML coverage. Increasing the NiO coverage further to 28 ML leads only to incidental shifts of the spectral features noted in Fig. 8. These ELS results show that the electronic structure determined by ELS for NiO films with

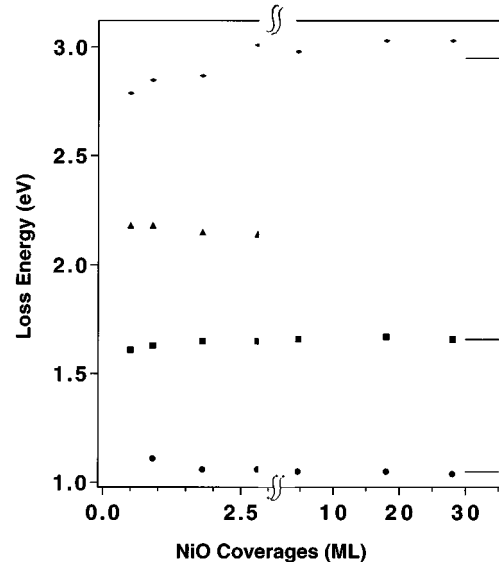


FIG. 8. Electron energy loss energies as a function of NiO coverage (thickness). The short solid lines on the figure indicate the corresponding values measured for single crystal NiO(100) (Ref. 27).

thicknesses between 2.8 and 28 ML supported on the MgO(100)/Mo(100) surface are essentially identical.

IV. DISCUSSION

A. Growth mode and thermal stability

Epitaxial growth occurs for all four mixed-oxide systems addressed in this study, i.e., NiO on MgO(100)/Mo(100), NiO on CaO(100)/Mo(100), MgO on NiO(100)/Mo(100) and CaO on NiO(100)/Mo(100). However, the degree of long-range order, reflected by the quality of the LEED data, is significantly different across the series. The MgO-NiO shows excellent long-range order with very sharp LEED images. The CaO-NiO system, on the other hand, exhibits rather poor long-range order as indicated by the diffuse LEED image and the elevated background signal. These differences in long-range order can be explained by noting the differences in lattice constants among this group of oxides. The oxides of Mg, Ca, and Ni exhibit the rocksalt structure; however, their lattice constants are significantly different (see Table I). The similar lattice constants of MgO and NiO facilitate epitaxial growth of MgO on NiO and NiO on MgO. Furthermore, the lattice constant of the Mo(100) surface is very similar to that of MgO or NiO, promoting the growth of high quality MgO(100) or NiO(100) films. In contrast, the large mismatch in the lattice constants between NiO and

TABLE I. Lattice Constants for NiO(100), MgO(100), CaO(100), and Mo(100).

NiO(100)	MgO(100)	CaO(100)	Mo(100)
2.947 Å	2.978 Å	3.402 Å	3.147 Å

CaO leads to significant strain at the NiO/CaO interface resulting in poor epitaxy of NiO on CaO and CaO on NiO.

The growth mode of an oxide overlayer A on an oxide substrate B is usually determined by the relative surface and cohesive energies of pure A (S_A), pure B (S_B) and the interface energy of A-B (S_{AB}). The fact that similar growth modes are observed for NiO on MgO(100) and MgO on NiO(100), and for CaO on NiO(100) and NiO on CaO(100), indicates very similar surface free energies for NiO, MgO and CaO. The excellent lattice match between MgO and NiO facilitates formation of the NiO-MgO interface without considerable strain. The Ni-O (or Mg-O) bond strength at the oxide interface is apparently comparable to the corresponding Ni-O (or Mg-O) bond in the bulk. On the other hand, a large lattice mismatch exists between CaO and NiO, thus leading to a large strain at the interface between NiO and CaO. This strain prevents ideal layer-by-layer growth of NiO on CaO(100) or CaO on NiO(100), and promotes the formation of 3D clusters at these interfaces.²⁰⁻²⁵

Although the growth modes are quite similar between MgO on NiO(100) and NiO on MgO(100), and between NiO on CaO(100) and CaO on NiO(100), the thermal stabilities of these systems are somewhat different. This behavior suggests that the thermal instability is due to interdiffusion, rather than clustering. The differences in thermal stability can be rationalized by considering the size differences of the relevant cations. For 1 ML of CaO on NiO, the diffusion of Ca into NiO would lead to substantial lattice strain within the NiO, since Ca^{2+} is significantly larger than Ni^{2+} . Accordingly, the highest thermal stability is observed for this system. For NiO on CaO, the interdiffusion of Ni and Ca is energetically favorable, since this mixing leads to strain relief within the CaO film due to the large lattice mismatch between CaO and the Mo(100) substrate. As a result, this system shows the lowest stability. Because of the similar cation sizes of Ni and Mg, the systems consisting of NiO and MgO display an intermediate stability between CaO/NiO(100) and NiO/CaO(100).

B. Electronic structure of oxide overlayers

The extensive investigations of the NiO(100) surface^{16,17,19-21} serve as a basis for our ELS studies. The intense peak at 4.6 eV in Fig. 7 has been assigned to the $\text{O}^{2-} 2p$ to $\text{Ni}^{2+} 3d$ charge transfer excitation.²⁶ The loss features below the optical band gap (~ 4 eV) of NiO have been shown to correspond to localized $d-d$ Ni^{2+} transitions.²¹ For single crystal NiO(100), Cox and Williams²⁰ observed peaks at 1.05, 1.66, 1.78, and 2.9 eV, and assigned these to the ${}^3A_{2g} \rightarrow {}^3T_{2g}$, ${}^3A_{2g} \rightarrow {}^1E_g$, ${}^3A_{2g} \rightarrow {}^3T_{1g}(F)$, and ${}^3A_{2g} \rightarrow {}^3T_{1g}(P)$ transitions, respectively. Moreover, Freitag et al.²¹ have studied NiO films grown epitaxially on Ni(100) as well as single crystal NiO(100) using ELS and *ab initio* calculations. These authors assigned the loss peaks at 1.1 and 1.87 eV to $d-d$ transitions of bulk NiO, while the losses at 0.57 and 1.62 eV were assigned to NiO surface states. These latter assignments were supported by noting energy shifts induced by the adsorption of NO.²¹ In the present work,

losses at 0.56, 1.05, 1.66, and 3.03 eV are observed for films thicker than 2.8 ML. As in the previous studies, the feature at 1.87 eV is apparent only as a peak asymmetry on the high energy side of the feature at 1.66 eV.

These results show that NiO films with thicknesses greater than 2.8 ML already exhibit an electronic structure identical to single crystal NiO(100). On the other hand, the electronic structure of thin NiO films (< 2 ML) on MgO(100) are quite different from that of bulk NiO(100). The loss feature at 1.1 eV was not detected for a 0.5 ML NiO film, consistent with previous assignments of this feature to a bulk transition. Instead, a new feature at 2.18 eV is apparent. This peak can be assigned either to an interface state or to a surface state not observed previously. Because of the similar lattice constants and ionicities of NiO and MgO, similar crystal fields should exist for the individual Ni ions in monolayer NiO on MgO compared to NiO on itself. Little change then is expected within the $d-d$ transitions for monolayer NiO on MgO compared to monolayer NiO on itself. Accordingly, the peak at 2.18 eV is assigned tentatively to a surface state.

For low NiO coverages, the loss features are shifted slightly from their bulk values as shown in Fig. 8. These shifts indicate a modification of the thin film NiO electronic structure by the MgO substrate. The modified electronic structure of submonolayer NiO on MgO(100) is related to the altered crystal field about the Ni^{2+} site. Since the lattice constant of NiO is slightly smaller than that for MgO, an elongation of the Ni-O bond parallel to the $\langle 100 \rangle$ direction is anticipated for submonolayer NiO. A contraction of the Ni-O bonds along the z -axis should accompany an expansion in the x - y plane. This distortion of the octahedral symmetry about the Ni^{2+} site splits the degeneracies of the d -levels, resulting in the electronic excitation levels moving either to higher or lower energies.

The difference in ionicities between NiO and MgO also plays an important role in defining the thin film properties of the NiO/MgO system. Since MgO is more ionic than NiO, the partial charge on the oxygen ion in MgO is somewhat larger than that on oxygen in NiO. This larger ionicity of the oxygen in MgO should compensate, to some extent, for the stretched Ni-O bond in the overlayer NiO on MgO, by increasing the crystal field along the z -axis.

V. CONCLUSION

Layered NiO-MgO and NiO-CaO films on Mo(100) and Mo(110) have been prepared and studied by AES, LEED, ISS, ELS, and NO-TPD. Epitaxial growth was found for NiO on MgO(100) and CaO(100); for MgO on NiO(100); and for CaO on NiO(100). The growth mode and thermal stability of the interface can be attributed to the differences in the relative lattice constants of the individual oxides and in the size of the various cations. Similar lattice constants facilitate layer-by-layer growth; large mismatches in lattice constants lead to substantial 3D clustering of the overlayer.

ACKNOWLEDGEMENTS

We acknowledge with pleasure the support of this work by the National Science Foundation under Contract No. DMR-9423707, and by Laboratory Directed Research and Development (LDRD) funding from Pacific Northwest Laboratories.

¹J. Nowotny, *Science of Ceramic Interface in Materials Science Monographs* (Elsevier, New York, 1993), Vol. 81.

²J. Nowotny, *Science of Ceramic Interface in Materials Science Monographs* (Elsevier, New York, 1991), Vol. 75.

³M. Ruehle, A. G. Evans, M. F. Ashby, and J. P. Hirth, *Metal-Ceramic Interfaces* (Pergamon, New York, 1990).

⁴H. H. Kung, *Transition Metal Oxides: Surface Chemistry and Catalysis* (Elsevier, New York, 1989).

⁵Y.-C. Xie and Y.-Q. Tang, *Adv. Catal.* **37**, 1 (1990).

⁶M.-C. Wu, J. S. Corneille, C. A. Estrada, J.-W. He, and D. W. Goodman, *Chem. Phys. Lett.* **182**, 472 (1991).

⁷J.-W. He, C. A. Estrada, J. S. Corneille, M.-C. Wu, and D. W. Goodman, *Surf. Sci.* **261**, 164 (1992).

⁸M.-C. Wu, C. A. Estrada, and D. W. Goodman, *Phys. Rev. Lett.* **67**, 2910 (1991).

⁹M.-C. Wu, C. A. Estrada, J. S. Corneille, and D. W. Goodman, *J. Chem. Phys.* **96**, 3892 (1992).

¹⁰M.-C. Wu, C. M. Truong, K. Coulter, and D. W. Goodman, *J. Am. Chem. Soc.* **114**, 7565 (1992).

¹¹M.-C. Wu, C. M. Truong, and D. W. Goodman, *Phys. Rev. B* **46**, 12688 (1992).

¹²J. S. Corneille, J.-W. He, and D. W. Goodman, *Surf. Sci.* **306**, 269 (1994).

¹³C. M. Truong, M.-C. Wu, and D. W. Goodman, *J. Chem. Phys.* **97**, 9447 (1992).

¹⁴M.-C. Wu, C. M. Truong, and D. W. Goodman, *J. Phys. Chem.* **97**, 4182 (1993).

¹⁵C. M. Truong, M.-C. Wu, and D. W. Goodman, *J. Am. Chem. Soc.* **115**, 3647 (1993).

¹⁶*Adsorption on Ordered Surfaces of Ionic Solids and Thin Films*, edited by H. J. Freund and E. Umbach (Springer, New York, 1993).

¹⁷C. Xu and D. W. Goodman in *Handbook of Heterogeneous Catalysis*, edited by G. Ertl, H. Knoezinger, and J. Weitkamp (in press).

¹⁸M.-C. Wu, C. M. Truong, and D. W. Goodman, *Phys. Rev. B* **46**, 12688 (1992).

¹⁹K. Akimoto, Y. Sakisaka, M. Nishijima, and M. Onchi, *J. Phys. C: Solid State Phys.* **11**, 2535 (1978).

²⁰P. A. Cox and A. A. Williams, *Surf. Sci.* **152/153**, 791 (1985).

²¹A. Freitag, V. Staemmler, D. Cappus, C. A. Ventrice, Jr., K. Al Shamery, H. Kuhlenbeck, and H.-J. Freund, *Chem. Phys. Lett.* **210**, 10 (1993).